RSC Advances

PAPER

View Article Online
View Journal | View Issue

Cite this: *RSC Adv.*, 2022, **12**, 36038

Fluorination effects on bithiophene unit in benzodithiophene-4,8-dione based D–A type alternating copolymers for highly efficient polymer solar cells†

Yunxiang Chen *[ab] and Fang Chen [a]

Received 20th September 2022
Accepted 3rd December 2022

DOI: 10.1039/d2ra05925h

rsc.li/rsc-advances

In this study, two D–A polymers consisting of benzodithiophene-4,8-dione and tetrathiophene with or without fluorination were synthesized to reveal the photovoltaic properties of fluorination effect on the polymer backbone. Polymer PDFTB with two fluorine atoms substituted on the backbone exhibits an enhanced π–π stacking effect, deeper HOMO energy level and better backbone planarity than PDTB without fluorine atom substitution. Devices based on PDFTB:ITIC show a power conversion efficiency of 4.39%, which is 15% higher than that of PDTB-based devices due to the higher hole mobility, optimized surface morphology and homogeneous phase separation of the active layer. These results suggest that the fluorination strategy is a facile way to design polymeric donors for solvent-processed polymer solar cells.

1. Introduction

In the quest for alternative energy sources, bulk-heterojunction (BHJ) polymer solar cells (PSCs) have been widely investigated due to their advantages of flexible, low-cost, and large-area printable techniques, such as roll-to-roll coating and inkjet printing.[1–8] Thanks to the development of material synthesis and device fabrication, significant progress in the power conversion efficiency (PCE) of BHJ-based PSC devices has been achieved. The BHJ active layer in PSCs consists of donor and acceptor materials. The compatibility of donor and acceptor materials may affect the phase separation scale and microstructure morphology of the BHJ films, and the energy levels of donor and acceptor can provide the driving force for charge separation.[9–15] Therefore, much attention has been paid to the design and optimization of donor and acceptor materials in recent years.

Developing D–A type alternating polymers has proved to be an effective way to realize high-performance PSC devices, due to the occurrence of the intramolecular charge transport (ICT) effect.[16–19] However, molecular design still plays an important role in promoting photovoltaic properties of polymeric donors. Broad light absorption and suitable energy levels are the fundamental requirements of high-performance donor materials. Molecular energy levels including LUMO and HOMO levels can be adjusted by adding electron-donating or electron-accepting units on the polymer backbone. Electron-accepting units like cyano groups and fluorine atoms are popularly used to downshift the molecular energy levels of donor materials, in order to boost the open-circuit voltage (V_{OC}) of devices.[20–22] In addition, introducing fluorine atoms to the polymer backbone also can enhance the ICT and π–π stacking effects, which may promote the short-circuit current density (J_{SC}) of PSC devices.[18]

To further investigate the fluorination effect on polymeric donor materials, two alternating conjugated polymers were designed and synthesized. Benzodithiophene-4,8-dione (BDD) was employed as the electron-accepting unit, which was then connected with either of two different electron-donating units, namely tetrathiophene and fluorinated tetrathiophene, to afford polymers named PDTB and PDFTB. Of the two medium-band-gap polymers, PDFTB with two fluorine atoms substituted on the polymer backbone shows promising device performance, realizing an average PCE of 4.11%, and a maximum value of 4.39% with V_{OC} of 0.86 V, and J_{SC} of 12.28 mA cm^{-2}. For the other polymer, PDTB, both V_{OC} and J_{SC} values experienced a dramatic decrease to 0.64 V and 9.91 mA cm^{-2} respectively, which resulted in a lower PCE of 3.81%. To reveal the fluorination effect on the structure-device performance relationships, photophysical/electrochemical properties, charge transport and BHJ film morphologies were investigated to provide a valuable design strategy for high-performance photovoltaic materials.

2. Experimental section

2.1. Materials and synthesis

All the starting materials were purchased from Nanjing Zhiyan Technology Co. Ltd. Acceptor ITIC was purchased from

[a]College of Materials and Chemical Engineering, Minjiang University, Fuzhou, 350007, PR China. E-mail: falling147@126.com

[b]Fujian Engineering and Research Center of New Chinese Lacquer Materials, Fuzhou, 350007, PR China

† Electronic supplementary information (ESI) available. See DOI: https://doi.org/10.1039/d2ra05925h

SunaTech Inc. Pd_2dba_3 and P(*o*-tol)$_3$ were purchased from Admas. Toluene was freshly distilled from CaH_2. Other solvents and reagents were used as received, unless otherwise specified.

2.1.1. Synthesis of 1,3-bis(2-ethylhexyl)-5,7-bis(4-(2-octyldodecyl)thiophen-2-yl)-4*H*,8*H*-benzo[1,2-*c*:4,5-*c*′]dithiophene-4,8-dione (3). 1,3-Dibromo-5,7-bis(2-ethylhexyl)-4*H*,8*H*-benzo[1,2-*c*:4,5-*c*′]dithiophene-4,8-dione (**1**) (500.0 mg, 0.831 mmol), Pd_2dba_3 (17 mg) and P(*o*-tol)$_3$ (22.7 mg) were added to a 100 mL flask. Following nitrogen flushing for 10 min, tributyl(4-(2-octyldodecyl)thiophen-2-yl)stannane (**2**) (1110 mg, 1.70 mmol) and dry toluene (30 mL) were injected to the mixture and stirred at 110 °C overnight. A saturated solution of KF (30 mL) was added into the reaction and stirred for another 6 h. After cooling to room temperature, the mixture was extracted with ethyl acetate (3 × 40 mL) followed by washing with saturated NaCl (50 mL). The organic phase was dried by anhydrous $MgSO_4$. After evaporating the solvent, the residue was purified by column chromatography on silica gel, employing petroleum ether : CH_2Cl_2 (8 : 1, v/v) as the eluent to afford the final product (538.9 mg) as a light-yellow oil. ^{1}H NMR (400 MHz, $CDCl_3$) δ 7.56 (d, J = 1.2 Hz, 1H), 7.06 (s, 1H), 3.31 (s, 2H), 2.56 (s, 2H), 1.83–1.72 (m, 1H), 1.70–1.62 (m, 1H), 1.40–1.21 (m, 40H), 0.97–0.81 (m, 12H).

2.1.2. Synthesis of 1,3-bis(5-bromo-4-(2-octyldodecyl)thiophen-2-yl)-5,7-bis(2-ethylhexyl)-4*H*,8*H*-benzo[1,2-*c*:4,5-*c*′]dithiophene-4,8-dione (4). 5,6-Difluoro-4,7-bis(4′-hexyl-3-(2-octyldodecyl)-[2,2′-bithiophen]-5 yl)benzo[1,2,5]thiadiazole (**5**) (538.9 mg, 0.460 mmol) and NBS (163.8 mg, 0.920 mmol) were added into a 50 mL round-bottom flask, which then charged with nitrogen three times. Then, $CHCl_3$ (20 mL) was injected into the mixture. The reaction was stirred at 0 °C for 1 h. After removing the solvent, the residue was purified by column chromatography, employing petroleum ether : CH_2Cl_2 (8 : 1, v/v) as the eluent to afford the final product (520.0 mg) as a light-yellow oil.

2.1.3. Synthesis of PDTB. Compound **4** (150 mg, 0.113 mmol) and 5,5′-bis(trimethylstannyl)-2,2′-bithiophene (**5a**) (59.65 mg, 0.113 mmol) were dissolved in freshly distilled toluene (20 mL), and Pd_2dba_3 (2.31 mg) and P(*o*-tol)$_3$ (3.09 mg) were added into the solution. After being flushed by nitrogen for 10 min, the reaction was stirred at 110 °C for 48 h. After cooling to room temperature, the mixture was precipitated into methanol to afford the crude polymer. The crude polymer was purified by Soxhlet extraction *via* methanol, acetone and hexane and collected by chloroform. Finally, the polymer was precipitated into methanol, and dried under vacuum to afford the polymer PDTB (99.8 mg). M_n = 12.1 kDa, PDI = 1.71. Decomposition temperature (5% weight loss): 430 °C. ^{1}H NMR (400 MHz, $CDCl_3$) δ 7.66 (s, 1H), 7.20 (d, J = 4.4 Hz, 2H), 3.36 (s, 2H), 2.80 (s, 2H), 1.81 (s, 2H), 1.40–1.22 (m, 40H), 0.97–0.80 (m, 12H).

2.1.4. Synthesis of PDFTB. The synthetic procedure was the same as for PDTB. The number-average molecular weight (M_n) = 14.7 kDa, polydispersity index (PDI) = 2.03. Decomposition temperature (T_d) (5% weight loss): 426 °C. ^{1}H NMR (400 MHz, $CDCl_3$) δ 7.50 (dd, J = 10.2, 3.1 Hz, 1H), 7.00 (s, 1H), 3.33 (s, 2H), 2.77 (s, 2H), 1.78 (s, 2H), 1.25 (d, J = 3.4 Hz, 40H), 0.84 (t, J = 6.4 Hz, 12H).

2.2. Fabrication and characterization of devices

The PSC devices were fabricated with a conventional device structure of ITO/PEDOT:PSS/polymer:$PC_{71}BM$/LiF/Al. Patterned ITO glass (15 Ω per square) was cleaned in an ultrasonic bath of detergent, deionized water, acetone and isopropyl alcohol. All the ITO glass were treated in an ultraviolet-ozone plasma for 15 min before use in fabrication. Poly(3,4-ethylenedioxythiophene):poly(styrenesulfonate) (PEDOT:PSS) (Clevios P, VP AI 4083) was spin-coated on to the ITO surface and annealed for 15 min to form a thin film at about 30 nm. The total concentration of polymer and ITIC in chloroform was 10 mg mL^{-1} and the solutions were stirred at 30 °C overnight. The solutions were heated to 50 °C and stirred for another 20 min before spin-coating to ensure solubility. The solutions were spin-coated onto the PEDOT:PSS layer to form the active layers, the thickness being determined by an Alpha Step D-300 as about 100 nm. LiF (1 nm) and Al (100 nm) were deposited by vacuum evaporation under 3 × 10^{-4} Pa to form the electron-transporting layer and cathode respectively. The active area of the cells was 0.04 cm^2. Current–voltage (*J*–*V*) curves were measured under 100 mW cm^{-2} irradiation by using the simulated solar light from a Newport Orial solar 3A simulator and recorded with a Keithley 2400 source meter. External quantum efficiencies (EQEs) were measured with an Enlitech QE-R system. For space-charge-limited current (SCLC) method, architectures of hole-only devices and electron-only devices were ITO/PEDOT:PSS/polymer:$PC_{71}BM$/MoO_3/Ag and ITO/PFN/polymer:$PC_{71}BM$/PFN/Al respectively.

2.3. Materials characterization and measurements

^{1}H NMR spectra were obtained with a Bruker AVIII-400 spectrometer. All the intermediates and polymers were tested in $CDCl_3$ solution and tetramethylsilane as standard. UV-visible absorption spectra were measured with a Shimadzu UV-2600 spectrophotometer. All solution experiments were conducted in dilute chloroform. Cyclic voltammetry (CV) measurements were performed on a Zahner IM6e electrochemical workstation with a scan rate of 0.1 V s^{-1}. Glassy carbon electrode and platinum electrode were used as working electrode and counter electrode respectively. Silver wire coated with silver chloride (Ag/AgCl) electrode was used as reference electrode. CV measurements were carried out in an electrolyte solution of acetonitrile containing 0.1 M *n*-Bu_4NPF_6. Polymer films were deposited from chloroform solution onto the working electrodes. Fc/Fc$^+$ was used as internal standard. The absolute energy level of Fc/Fc$^+$ was −4.80 eV. The solution was bubbled with nitrogen before the measurements. The potential of the polymers was corrected by the standard reference of Fc/Fc$^+$ (0.40 V *vs.* Ag/Ag$^+$ electrode). Highest occupied molecular orbital (HOMO) and lowest unoccupied molecular orbital (LUMO) energy levels were calculated from the onset oxidation potential according to the following equations: $E_{HOMO} = -(4.40 + E_{ox}^{onset})$ eV; $E_{LUMO} = -(4.40 + E_{red}^{onset})$ eV. Energy levels were estimated from the optical band gap and HOMO levels. Gel permeation chromatography (GPC) was performed using a waters 1515 at 40 °C with tetrahydrofuran as eluent against

polystyrene standard. Differential scanning calorimetry (DSC) was conducted with a NETZSCH DSC 214 nevio, under a nitrogen atmosphere at a heating rate of 10 °C min^{-1}. Thermogravimetric analysis (TGA) was performed with a Mettler-Toledo 851e/822e analysis system under a nitrogen atmosphere at a heating rate of 10 °C min^{-1}. Photoluminescence (PL) was measured by a RF-5301PC spectrometer. X-ray diffraction (XRD) was conducted using an X'Pert3 and Empyrean in reflection mode. Atomic force microscopy (AFM) images were obtained using a Bruker dimension edge scanning probe microscope in tapping mode. Transmission electron microscopy (TEM) images were obtained using a JEOL-2000 FX electron microscope at a voltage of 200 kV.

3. Results and discussion

3.1. Synthesis and characterization

The chemical structures and synthetic route of the polymers are shown in Fig. 1. 1,3-Bis(2-ethylhexyl)-5,7-bis(4-(2-octyldodecyl) thiophen-2-yl)-4*H*,8*H*-benzo[1,2-*c*:4,5-*c*′]dithiophene-4,8-dione (**3**) was obtained by Stille coupling reaction between 1,3-dibromo-5,7-bis(2-ethylhexyl)-4*H*,8*H*-benzo[1,2-*c*:4,5-*c*′]dithiophene-4,8-dione (**1**) and tributyl(4-(2-octyldodecyl)thiophen-2-yl)stannane (**2**), with Pd_2dba_3 as the catalyst and P(*o*-tol)$_3$ as the ligand in toluene at 110 °C. NBS bromination was carried out in chloroform to afford 1,3-bis(5-bromo-4-(2-octyldodecyl)thiophen-2-yl)-5,7-bis(2-ethylhexyl)-4*H*,8*H*-benzo[1,2-*c*:4,5-*c*′]dithiophene-4,8-dione (**4**). Polymers PDTB and PDFTB were synthesized *via* Stille coupling reaction between **4** and 5,5′-bis(trimethylstannyl)-2,2′-bithiophene (**5a**) or (3,3′-difluoro-[2,2′-bithiophene]-5,5′-diyl)bis(trimethylstannane) (**5b**). PDTB and PDFTB exhibit good solubility in common organic solvents, for example chloroform and 1,2-dichlorobenzene. GPC analysis of the two polymers showed M_n of PDTB and PDFTB are 12.1 and 14.7 kDa respectively. The corresponding PDI were calculated as 1.74 and 2.03. DSC measurements (Fig. S1 in the ESI†) of the two polymers reveal that no obvious endothermic processes were observed in the range of 30–300 °C. The resulting polymers show a high glass transmission temperature (T_g) of around 270 °C. The decomposition temperatures (T_d) of PDTB and PDFTB are confirmed to be 388 and 402 °C respectively at 5% weight loss, which are obtained from TGA (Fig. S2 in the ESI†). The excellent thermal stabilities of the polymers establish their application potential in photovoltaic devices.

3.2. Physical and electrochemical properties of polymers

The normalized UV-visible absorption spectra of PDTB and PDFTB in dilute chloroform are shown in Fig. 2a. Both polymers show two distinct absorption bands. The absorption band in the high-energy region of 350–450 nm may be attributed to the localized π–π* transition, while the band located in the low-energy region of 470–600 nm indicated ICT from electron-donating unit to electron-accepting unit. When going from solution to solid state (Fig. 2b), the two absorption bands show a red shift, implying the increased π–π stacking of polymer

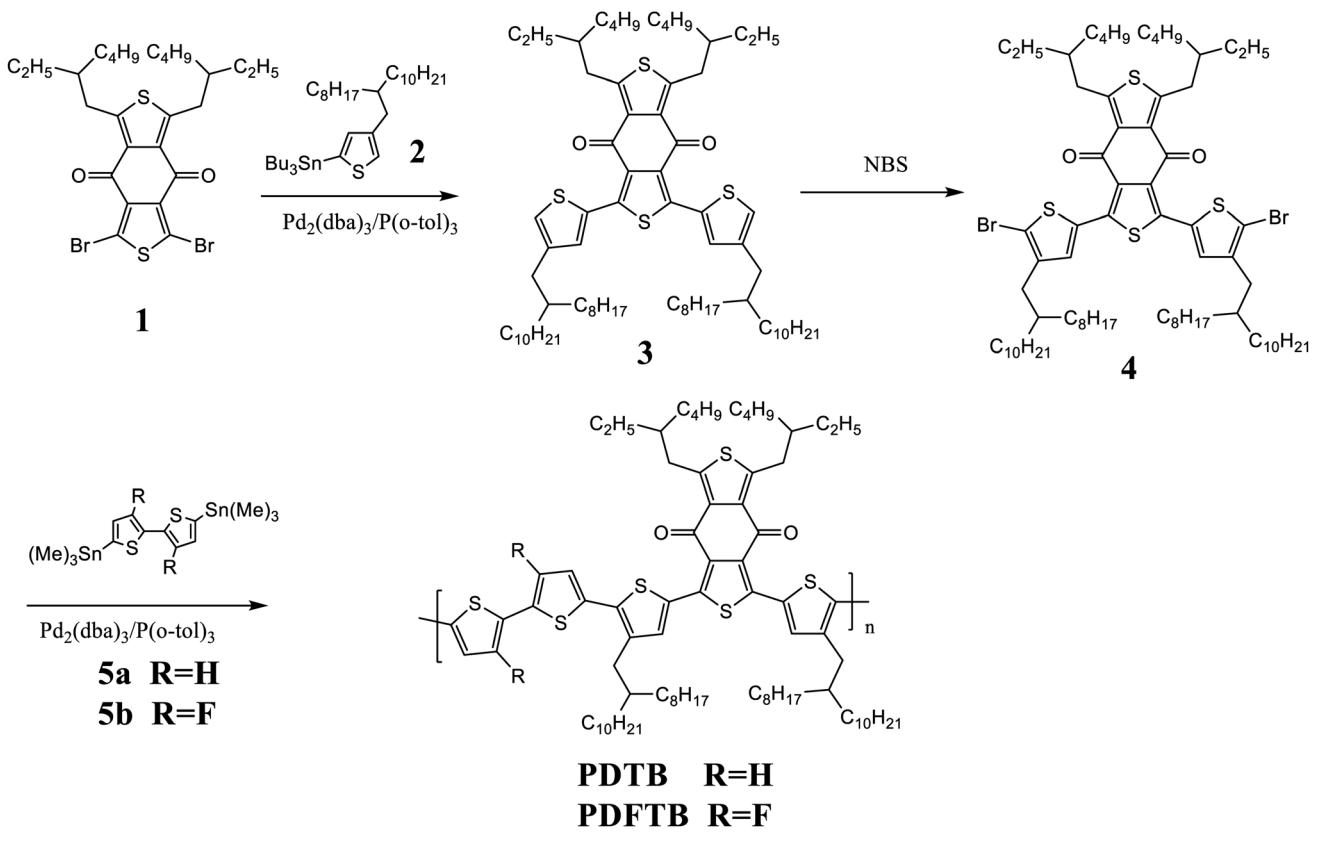

Fig. 1 Synthetic route and chemical structures of PDTB and PDFTB.

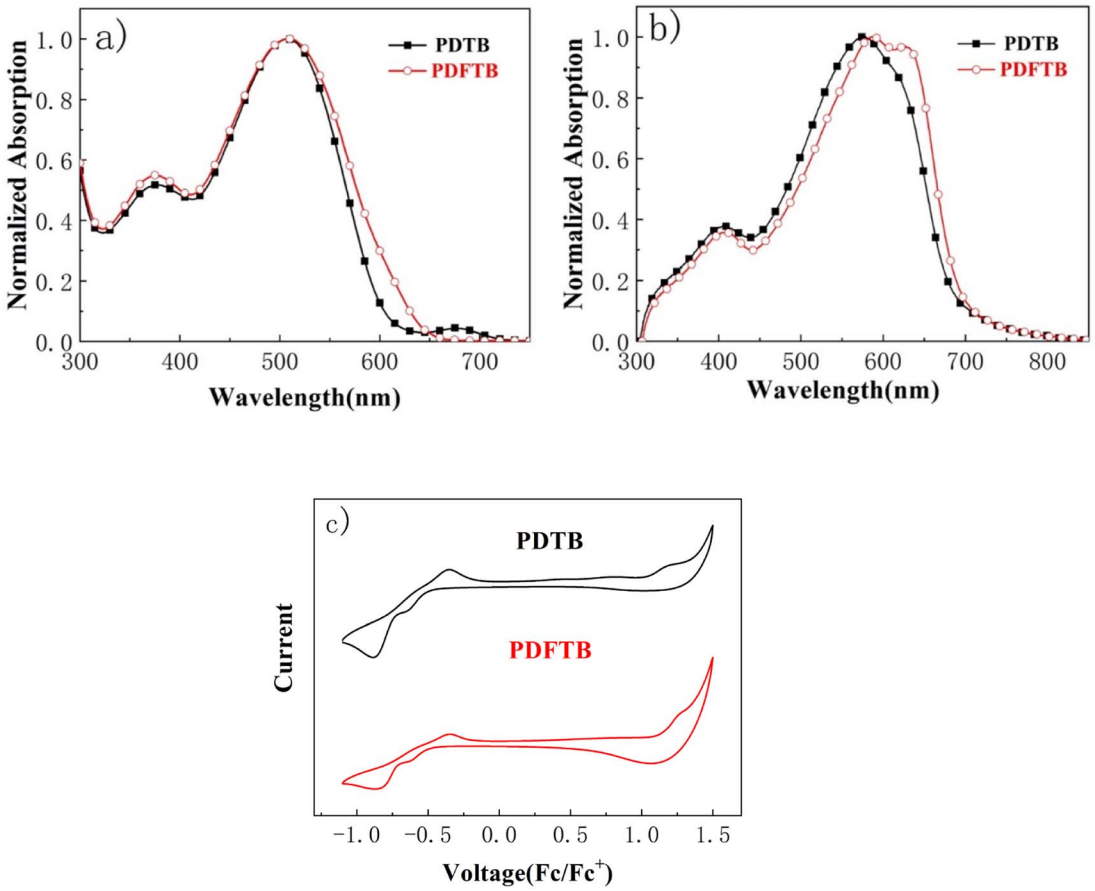

Fig. 2 UV-visible absorption spectra of PDTB and PDFTB in (a) chloroform and (b) solid state, and (c) CV curves of PDTB and PDFTB films.

backbone. PDFTB exhibits a vibronic absorption shoulder at around 660 nm in the solid state, implying that the introduction of fluorine atoms on the polymer backbone enhanced the interchain interaction and strong stacking among the polymer chains.[21,23] Moreover, PDFTB shows a red-shifted maximum absorption peak in comparison with the non-fluorinated polymer, which may benefit the light-harvesting of low-energy photons and lead to an improvement of J_{SC} for solar cell devices. The absorption onset (λ_{onset}) of PDTB in the solid state is determined to be 691 nm; when fluorine atoms are introduced into the polymer backbone, the absorption onset of PDFTB shows a slight blue shift to 687 nm. This is attributed to the electron-withdrawing effect of the fluorine atoms, which weakens the conjugation strength.[21,24] The optical bandgaps (E_g^{opt}) of PDTB and PDFTB are calculated to be 1.79 eV and 1.80 eV, respectively.

The frontier energy levels of the two polymers were investigated by CV measurements. The LUMO energy levels of PDTB and PDFTB were determined to be −3.69 eV and −3.74 eV, while the HOMO energy levels were determined to be −5.58 eV, and −5.68 eV for PDTB and PDFTB, respectively. The fluorinated polymer PDFTB displays both deeper LUMO and HOMO energy levels than PDTB. This may be attributed to the electron-withdrawing effect of the fluorine atoms. Accordingly, the electronic band gaps of PDTB and PDFTB were calculated from CV measurements as 1.89 eV and 1.94 eV, respectively. The physical and optical properties and frontier energy levels of PDTB and PDFTB are summarized in Table 1.

Density functional theory (DFT)-based calculations were conducted to further investigate the fluorination effect on the polymer backbone, for which alkyl side chains are truncated to a methyl for simplification (Fig. 3a). For the two polymers, the dihedral torsion angle between the BDD unit and the adjacent thiophene ring (θ_1) is calculated to be around 21°, because of the steric hindrance of the carbonyl group on the BDD unit.[25] The dihedral angles between the thiophene rings (θ_2 and θ_3) for

Table 1 Molecular weights, decomposition temperatures, optical properties and frontier energy levels of PDTB and PDFTB

Polymer	M_n (kDa)	PDI	T_d (°C)	λ_{onset} (nm)	E_g^{opt} (eV)	E_{HOMO} (eV)	E_{LUMO} (eV)	E_g^{CV} (eV)
PDTB	12.1	1.74	388	691	1.79	−5.58	−3.69	1.89
PDFTB	14.7	2.03	402	687	1.80	−5.68	−3.74	1.94

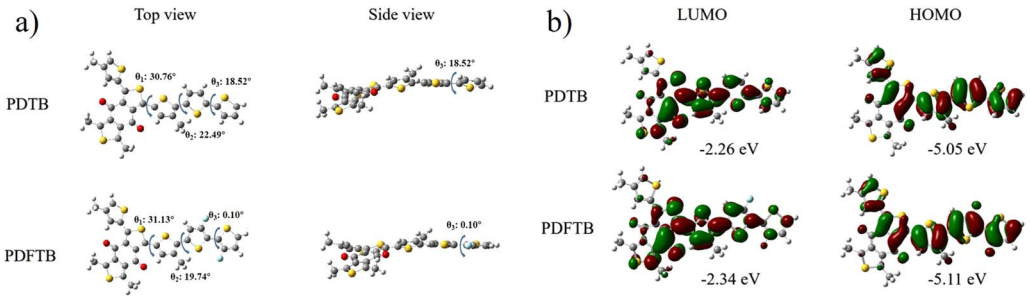

Fig. 3 Geometries of triads of repeating units of polymers by DFT calculation (a), orbital distribution (b).

polymer PDTB are 22.49° and 18.52° respectively. After the fluorine atoms are inserted into the polymer backbone, the corresponding dihedral angles between the thiophene rings of PDFTB decrease dramatically to 19.74° and 0.10° respectively, indicating that the fluorine substitution may build up the non-covalent conformation locks between sulfur and fluorine atoms.[21] This can effectively reduce the steric hindrance between the thiophene rings in order to improve the backbone planarity, π–π stacking effect and the molecular packing, which can improve the charge transfer ability of the polymeric donor. When observing the orbital distribution (Fig. 3b), it is evident that the HOMO is occupied by the fluorine atoms in PDFTB. Compared with PDTB, the fluorination lowers the HOMO/LUMO level of PDFTB, which is in accordance with the CV measurements.

3.3. Photovoltaic properties of the polymers

Polymers PDTB and PDFTB were used as donors in PSC devices with the conventional device architecture of ITO/PEDOT:PSS/polymer:ITIC/LiF/Al to evaluate the effect of fluorination on the polymer backbone. The devices were tested under illumination of AM 1.5G simulated solar light. BHJ active layers were spin-coated with chloroform. In order to achieve maximum PCE, we optimized the devices by modifying D : A ratios, solvent additives and thermal annealing process. The optimal D : A weight ratio was identified as 1 : 1 after checking the weight ratios from 1 : 0.8 to 1 : 1.2; the optimization details are available in Table S1.† The devices that were processed with 1,8-diiodooctane (DIO) as additive followed by thermal annealing at 100 °C for 10 min exhibited further promotion of PCE compared with the devices processed without additives; the optimization details are available in Table S2.† The optimal PCE of the devices fabricated with PDTB was obtained as 3.81% with photovoltaic parameters $V_{OC} = 0.64$ V, $J_{SC} = 9.91$ mA cm^{-2}, FF = 60.1%. The fluorinated polymer PDFTB exhibited a higher PCE of 4.39%. *J–V* curves of PDTB:ITIC- and PDFTB:ITIC-based PSC devices are shown in Fig. 4a. The photovoltaic parameters are summarized in Table 2. The enhancement resulted from the improvement of V_{OC} and J_{SC} despite the slightly lower FF. The fluorine substituents downshifted the HOMO level of the polymeric donor, which demonstrated higher V_{OC} of the devices. Moreover, fluorine substitution improved the intermolecular interaction, which may lead to better charge mobilities and J_{SC}. EQE spectra were obtained to evaluate the spectral responses of the devices. EQE spectra of the PSC devices are shown in Fig. 4b. Both PDTB- and PDFTB-based PSC devices showed maximum photoresponses in the range 550–700 nm. The photocurrent densities calculated from integrating the EQE spectra were 9.32 and 12.69 mA cm^{-2}, which are consistent with the J_{SC} values obtained from the *J–V* measurements.

3.4. Charge transport properties

In order to study the charge transport properties of polymer:-ITIC blends, the SCLC method was conducted to measure the

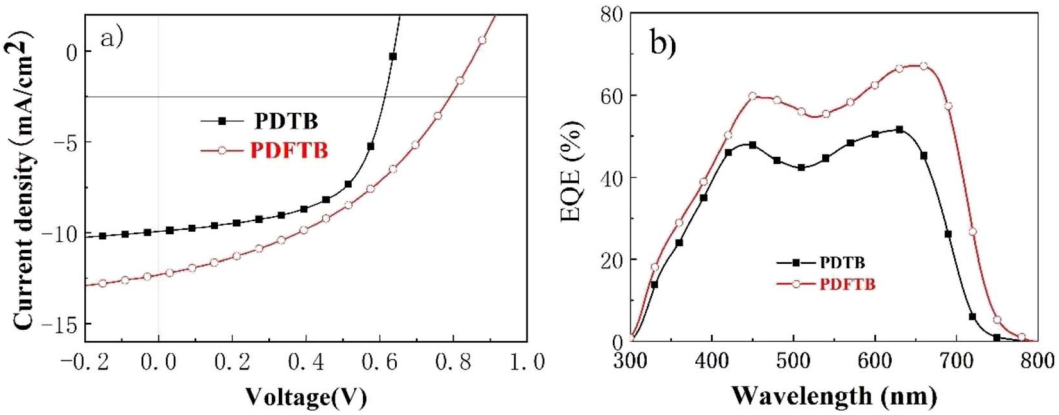

Fig. 4 *J–V* characteristics (a) and EQE spectra (b) of PDTB:ITIC- and PDFTB:ITIC-based PSC devices.

Table 2 Photovoltaic parameters of polymer:ITIC-based PSC devices

Polymer	V_{OC} (V)	J_{SC} (mA cm^{-2})	FF (%)	PCE[a] (%)
PDTB	0.64	9.91	60.1	3.81/3.58
PDFTB	0.86	12.28	41.5	4.39/4.11

[a] The value stands for the maximum/average PCE obtained from no less than 10 devices.

hole mobility (μ_h) and electron mobility (μ_e) of the PSCs. Hole-only devices were fabricated with the device structure of ITO/PEDOT:PSS/active layer/MoO_3/Ag, and electron-only devices were fabricated with the configuration of ITO/PFN/active layer/PFN/Al. The *J–V* curves are shown in Fig. 5. The PDTB:ITIC blend film exhibited μ_h and μ_e of 1.643×10^{-5} cm^2 V^{-1} s^{-1} and 1.009×10^{-5} cm^2 V^{-1} s^{-1}, respectively. The PDFTB:ITIC blend film exhibited relatively higher μ_h and μ_e of 2.170×10^{-5} cm^2 V^{-1} s^{-1} and 1.033×10^{-6} cm^2 V^{-1} s^{-1} respectively. Although the PDFTB:ITIC film exhibited higher mobilities, which may lead to a higher J_{SC}, the PDFTB:ITIC blend film showed relatively unbalanced charge transport ability (μ_h/μ_e = 2.1) compared with the PDTB:ITIC film (μ_h/μ_e = 1.6). The relatively unbalanced hole and electron mobilities may cause bimolecular recombination, which may decrease the FF of PDFTB:ITIC-based devices.[26]

3.5. Morphology characteristics

The π-π stacking characteristics of polymer:ITIC blend films were studied by XRD analysis. The curves are shown in Fig. 6. The broad diffraction peak of PDFTB:ITIC film shows a slight increase compared with the PDTB:ITIC film at around 2θ = 23.5°, indicating the enhancement of the π–π stacking, which is consistent with UV-visible spectra and DFT calculations. According to a previous report, the enhancement can reduce the distance of polymer chains and facilitate charge transport, which may lead to an improvement of photocurrent and J_{SC} of the devices.[27]

PL spectra of neat polymer films and polymer:ITIC blend films were obtained to investigate the exciton dissociation characteristics. All films were excited at 525 nm and PL spectra are shown in Fig. 7. PDTB and PDFTB neat films show PL emission from about 620 to 850 nm. For the blend films, PL emissions are greatly suppressed in the emission wavelength, which indicates that the excitons generated in the donor phase can effectively dissociate in the BHJ.

Surface morphologies of the polymer:ITIC blend films were investigated by AFM in tapping mode and TEM. The blend films were prepared with donor and acceptor according to the best performance devices. The images are shown in Fig. 8. The PDTB:ITIC blend film exhibits a relatively rough surface with a root mean square (RMS) roughness of 3.32 nm (Fig. 8a). The light and dark regions in the TEM images are normally assigned as donor-rich and acceptor-rich domains.[28] A large-scale phase separation can be observed in Fig. 8c, which may hinder the charge transport from donor to acceptor.[11] The PDFTB:ITIC blend film presented a smoother surface with a much lower RMS of 1.81 nm compared with the PDTB:ITIC film (Fig. 8b). The domain size was reduced and a suitable phase separation with nanoscale interpenetrating network structure can be found in the PDFTB:ITIC blend film (Fig. 8d) which provide channels for charge transportation.[29] The homogeneous phase

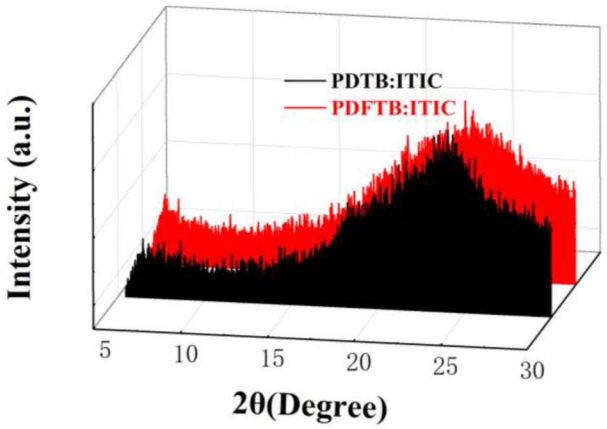

Fig. 6 XRD curves of polymer:ITIC blend films.

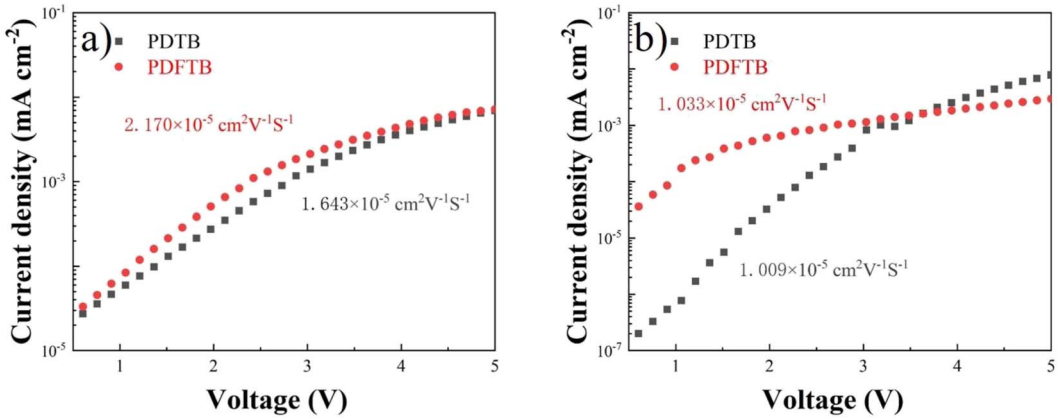

Fig. 5 *J–V* curves for hole-only (a) and electron-only (b) devices of polymer:ITIC-based devices.

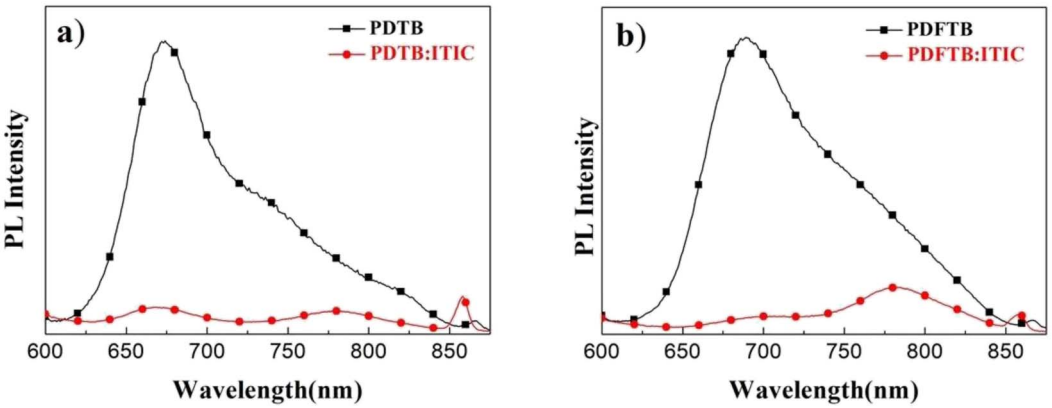

Fig. 7 PL spectra of neat films and polymer:ITIC blend films.

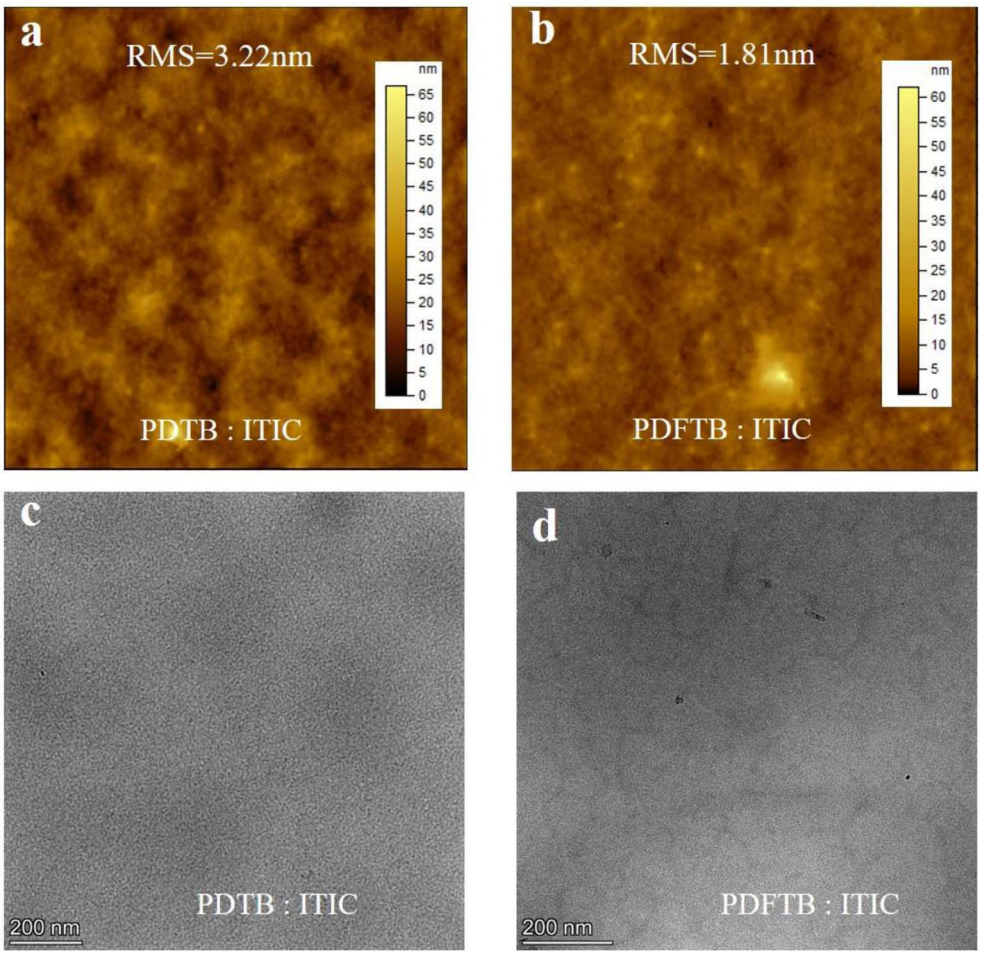

Fig. 8 (a, b) AFM and (c, d) TEM images of PDTB:ITIC and PDFTB:ITIC blend films.

separation indicates good miscibility between PDFTB and ITIC, which contributes to exciton dissociation, charge separation and transport and promotes J_{SC} of the devices.[18,30] The AFM and TEM images reveal that fluorination on the polymer backbone can effectively promote the surface morphology and the miscibility between donor and acceptor simultaneously, which may be favorable for higher J_{SC}.

4. Conclusion

In conclusion, two polymers based on BDT and tetrathiophene units have been synthesized with or without fluorine atoms on the backbone. When blended with ITIC, the fluorinated polymer PDFTB-based device exhibited dramatically enhanced V_{OC} and J_{SC}. The resulting device shows a PCE of 4.39% despite the

decrease of FF, which is 15% higher than that of the device based on non-fluorinated polymer PDTB. The enhancement of V_{OC} may be attributed to the deepened HOMO level through the fluorination strategy. Moreover, due to the substitution of fluorine atoms, the light-harvesting, π–π stacking and charge transport of the active layer were enhanced. Together with the optimal surface morphology of the PDFTB:ITIC film, these properties explained the boost of J_{SC}. However, the unbalanced charge transport ability may result in a lower FF. Our results demonstrated that the fluorination strategy is a promising way to fine-tune the absorption range, band gap and charge transport behavior of conjugated polymers, which is crucial for the enhancement of PSC performance.

Conflicts of interest

There are no conflicts of interests to declare.

Acknowledgements

This work was financially supported by the Natural Science Foundation of Fujian Province (2020J05171), the Education and Scientific Research Foundation of Fujian Province (JAT190601), Social Development Project of Fuzhou (2021-S-233), and Scientific Research Projects of Introduced Talents of Minjiang University (MJY21044).

References

1 M. Zhang, Y. Gu, X. Guo, F. Liu, S. Zhang, L. Huo, T. P. Russell and J. Hou, *Adv. Mater.*, 2013, **25**, 4944–4949.
2 C. Cui, W.-Y. Wong and Y. Li, *Energy Environ. Sci.*, 2014, **7**, 2276–2284.
3 T.-H. Lai, I. Constantinou, C. M. Grand, E. D. Klump, S. Baek, H.-Y. Hsu, S.-W. Tsang, K. S. Schanze, J. R. Reynolds and F. So, *Chem. Mater.*, 2016, **28**, 2433–2440.
4 S. Yang, Z. Lin, J. Wang, Y. Chen, Z. Liu, E. Yang, J. Zhang and Q. Ling, *ACS Appl. Mater. Interfaces*, 2018, **10**, 15980–15987.
5 L. Hong, H. Yao, Z. Wu, Y. Cui, T. Zhang, Y. Xu, R. Yu, Q. Liao, B. Gao, K. Xian, H. Y. Woo, Z. Ge and J. Hou, *Adv. Mater.*, 2019, **31**, e1903441.
6 J. Yang, P. Cong, L. Chen, X. Wang, J. Li, A. Tang, B. Zhang, Y. Geng and E. Zhou, *ACS Macro Lett.*, 2019, **8**, 743–748.
7 H. Liu, J. Wu, Y. Fu, B. Wang, Q. Yang, G. D. Sharma, M. L. Keshtov and Z. Xie, *Thin Solid Films*, 2021, **718**, 138486.
8 X. Li, X. Liu, P. Sun, Y. Feng, H. Shan, X. Wu, J. Xu, C. Huang, Z.-K. Chen and Z.-X. Xu, *RSC Adv.*, 2017, **7**, 17076–17084.
9 D. Baran, R. S. Ashraf, D. A. Hanifi, M. Abdelsamie, N. Gasparini, J. A. Rohr, S. Holliday, A. Wadsworth, S. Lockett, M. Neophytou, C. J. M. Emmott, J. Nelson, C. J. Brabec, A. Amassian, A. Salleo, T. Kirchartz, J. R. Durrant and I. McCulloch, *Nat. Mater.*, 2017, **16**, 363–369.
10 S. Dai, F. Zhao, Q. Zhang, T.-K. Lau, T. Li, K. Liu, Q. Ling, C. Wang, X. Lu, W. You and X. Zhan, *J. Am. Chem. Soc.*, 2017, **139**, 1336–1343.
11 W. Chen, H. Jiang, G. Huang, J. Zhang, M. Cai, X. Wan and R. Yang, *Sol. RRL*, 2018, **2**, 1800101.
12 Z. Wang, G. Han, L. Zhu, Y. Guo, Y. Yi, Z. Shuai and Z. Wei, *Phys. Chem. Chem. Phys.*, 2018, **20**, 24570–24576.
13 Z. Zhou, S. Xu, J. Song, Y. Jin, Q. Yue, Y. Qian, F. Liu, F. Zhang and X. Zhu, *Nat. Energy*, 2018, **3**, 952–959.
14 Y. J. Kim, E. S. Ahn, M. C. Hwang, C. E. Park and Y.-H. Kim, *Thin Solid Films*, 2016, **603**, 165–172.
15 K. Wang, S. Dong, X. Chen, P. Zhou, K. Zhang, J. Huang and M. Wang, *RSC Adv.*, 2020, **10**, 38344–38350.
16 M. Jeong, S. Chen, S. M. Lee, Z. Wang, Y. Yang, Z.-G. Zhang, C. Zhang, M. Xiao, Y. Li and C. Yang, *Adv. Energy Mater.*, 2018, **8**, 1702166.
17 X. Bao, Y. Zhang, J. Wang, D. Zhu, C. Yang, Y. Li, C. Yang, J. Xu and R. Yang, *Chem. Mater.*, 2017, **29**, 6766–6771.
18 B. A. Abdulahi, X. Li, M. Mone, B. Kiros, Z. Genene, S. Qiao, R. Yang, E. Wang and W. Mammo, *J. Mater. Chem. A*, 2019, **7**, 19522–19530.
19 S. Oh, D. H. Kim, T. Ahn and S. K. Lee, *J. Nanosci. Nanotechnol.*, 2018, **18**, 7221–7224.
20 N. Wang, Z. Chen, W. Wei and Z. Jiang, *J. Am. Chem. Soc.*, 2013, **135**, 17060–17068.
21 G. P. Kini, J. Y. Choi, S. J. Jeon, I. S. Suh and D. K. Moon, *Polymer*, 2018, **148**, 330–338.
22 D. Tu, X. Liu, J. Zhang, Q. Yang, S. Yu, X. Guo and C. Li, *ACS Sustainable Chem. Eng.*, 2018, **6**, 16005–16010.
23 J. W. Jo, J. W. Jung, E. H. Jung, H. Ahn, T. J. Shin and W. H. Jo, *Energy Environ. Sci.*, 2015, **8**, 2427–2434.
24 W. T. Neo, K. H. Ong, T. T. Lin, S.-J. Chua and J. Xu, *J. Mater. Chem. C*, 2015, **3**, 5589–5597.
25 D. Liu, J. Wang, C. Gu, Y. Li, X. Bao and R. Yang, *Adv. Mater.*, 2018, **30**, 1705870.
26 G. Li, V. Shrotriya, J. Huang, Y. Yao, T. Moriarty, K. Emery and Y. Yang, *Nat. Mater.*, 2005, **4**, 864–868.
27 Y. Li, L. Duan, D. Liu, W. Chen, X. Bao, H. Zhen, H. Liu and R. Yang, *J. Mater. Chem. C*, 2018, **6**, 2806–2813.
28 X. Ma, W. Gao, J. Yu, Q. An, M. Zhang, Z. Hu, J. Wang, W. Tang, C. Yang and F. Zhang, *Energy Environ. Sci.*, 2018, **11**, 2134–2141.
29 Y. Chen, G. You, D. Zou, Q. Zhuang, H. Zhen and Q. Ling, *Sol. Energy*, 2019, **183**, 350–355.
30 R. Peng, H. Guo, J. Xiao, G. Wang, S. Tan, B. Zhao, X. Guo and Y. Li, *ACS Appl. Energy Mater.*, 2018, **1**, 2192–2199.